Available online at www.sciencedirect.com
SCIENCE DIRECT®
Polymer 44 (2003) 5397–5406
polymer
www.elsevier.com/locate/polymer

Processing-structure-property investigation of blown HDPE films containing both machine and transverse direction oriented lamellar stacks

David Godshall[a], Garth Wilkes[a,*], Rajendra K. Krishnaswamy[b], Ashish M. Sukhadia[b]

[a]*Polymer Materials and Interfaces Laboratory, Department of Chemical Engineering, Virginia Tech, Blacksburg, VA 24061, USA*
[b]*Chevron Phillip Chemical Company LP, Bartlesville, OK 74004, USA*

Received 27 November 2002; received in revised form 14 April 2003; accepted 16 April 2003

Abstract

A series of blown films were prepared using two high density polyethylene resins of differing molecular weight and molecular weight distribution, using a high stalk process. Both the resins were processed at three frost line heights (FLHs) and three draw down ratios to determine the effect of processing parameters and resin characteristics on final film morphology and mechanical properties. By changing the FLH and the time to initiate transverse direction (TD) expansion, the relative number of lamellae stacked both perpendicular and parallel to the machine direction (MD) could be controlled for a constant blow up ratio (BUR) of 4:1. It was determined that the proportion of lamellae stacked parallel to the MD increased with increasing FLH. This effect was found to be related to the relaxation behavior of the melt and bubble shape. Increasing the stress in the stalk region was observed to lead to a reduction in stalk diameter just prior to bubble expansion, resulting in a greater effective BUR. Film morphology was observed to strongly influence end mechanical properties. Elmendorf tear resistance was found to increase in the MD and decreased in the TD with increasing FLH. The dart impact strength of these films was characterized with the surprising result that for one of the two resins studied, the dart impact increased with decreasing film gauge.

Keywords: Polyethylene; Blown film

1. Introduction

High density polyethylene (HDPE) films are used in numerous packaging applications where resistance to tear propagation and puncture are key attributes. As anticipated, the mechanical response of an HDPE film is a strong function of its morphological texture. This structure, in turn, is controlled by a combination of the melt process variables and the molecular characteristics of the resin [1–15]. In blown film, a planar, biaxial orientation promotes changes in the mechanical properties along both the machine direction (MD) and transverse direction (TD) of the film, relative to an isotropic sample. As well established in the literature, an imbalance of orientation within the film plane imparts a mechanical anisotropy, which may or may not be favored depending upon the requirements of the application. This directionally dependant response is, in turn, due to the anisotropic properties of individual crystalline lamellar stacks as well as the nature of the amorphous phase orientation. Recently, a review of the different modes of microstructural deformation for PE has been published [16]. As this recent review indicates, the stress–strain response of a uniaxially oriented HDPE film, with a stacked lamellar structure, stretched parallel to the lamellar long axes, tends to be dominated by the rigid, crystalline lamellae. In contrast, when deformation occurs perpendicular to the lamellar stacks (parallel to the lamellar normals), the mechanical properties of the film tend to be dominated by the softer amorphous material between lamellae, although the nature and concentration of tie molecules are also of importance. The response of the film to deformations at angles between these two extremes is more complicated, as bulk reorientation of the lamellae may occur (lamellar shear and rotation), and the yielding behavior of the crystals themselves is anisotropic (chain slip versus transverse slip etc.) [2,3,16–20]. These observations suggest that the presence of stacks of lamellae oriented in all directions within the film plane are necessary to achieve balanced mechanical properties in an oriented blown film.

As stated earlier, the orientation state of the final film is a

* Corresponding author.

0032-3861/03/$ - see front matter © 2003 Elsevier Ltd. All rights reserved.
doi:10.1016/S0032-3861(03)00349-5

function of both the processing history and the properties of the resin. The Keller–Machin (K–M) model [21,22], which has been used successfully by several authors, provides a starting point for the description of oriented, semi-crystalline morphologies in terms of row nucleated structures, and the mechanisms by which they are formed. The model states that under appropriate flow conditions, the chains with the longest relaxation times can become highly extended along the direction of flow if their Deborah number is greater than unity, where the Deborah number is defined as the ratio of a characteristic molecular relaxation time to the deformation time. Generally, those chains in the molecular weight distribution (MWD) with the longest relaxation times arise from the highest MW species or those that contain long chain branching (LCB). Upon orientation, the extended chains are the first to crystallize leading to the formation of fibril-nucleated structures. This results in an orientation of the crystalline *'c'* axis (chain axis) parallel to the deformation direction for the fibril nuclei. As the name implies, a fibril nucleus serves as a nucleating site for further, bulk crystallization. A second crystallization event produces lamellae nucleated by epitaxy from the oriented fibril nuclei. Note that the PE typically crystallizes into an orthorhombic unit cell, thus each axis of the unit cell is of unique length and perpendicular to the others. It is well known that the highest rate of chain folded crystallization, in the orthorhombic unit cell of PE, occurs along the *'b'* axis. This aniosotropic crystallization leads to preferential lamellar growth perpendicular to the fibril. The magnitude of *'b'* axis orientation relative to the flow direction, as well as *'a'* and *'c'* axis, are a function of the conditions of stress, or orientation, at the time of crystallization. It has been proposed by Choi et al. [1] that a biaxial melt deformation of HDPE can promote row structures oriented at various angles within the plane of the film. In addition, Sue et al. [2] has demonstrated that the bimodal lamellar populations, with their lamellar normals oriented perpendicular to each other, can be produced under certain blown film processing conditions. Based on the K–M model, it should be possible to control the relative amounts of lamellar stacks oriented in a given direction by manipulating the number and direction of fibril nuclei, through processing and resin variables, thus allowing for control of final film mechanical properties.

The formation of extended chains during flow is a consequence of the coil-stretch transition characteristic of macromolecules [22–25]. The coil-stretch transition occurs when the random coil conformation of a chain is perturbed by the flow around it. Planar flow geometries can be simplified by considering them to be composed of two components; rotational and extensional flows. The first component, rotational flow, causes individual fluid elements to tumble without leading to deformation. The second component, extensional flow, leads to deformation of the fluid element in the direction of extension. Simple shearing flows consist of equal parts rotational and elongational flows. It is for this reason that the shear flows are not as effective as purely extensional flows at creating high levels of molecular orientation. The susceptibility of a particular molecule to orientation by the extensional flow field is a function of the relative rates of extension and chain relaxation. Resistance to coil deformation arises from entropic driven elastic forces, associated with the thermally induced Brownian motion of the chains. These forces cause the coil to return to its unoriented state when outside of the flow field. In the blown film process, if the extended chains are given sufficient time prior to crystallization (initiated at the frost line), they may relax back to an unoriented, random coil state. Of course, a perturbation of the polymer coil will not occur unless the rate of deformation is greater than the rate at which the polymer chain can relax. Because the longest chains, with their greater number of entanglements and correspondingly longer relaxation times, are the most prone to produce fibril nuclei, it is important to understand how the MWD change can affect the interaction of a resin with the process.

A quantitative measure of melt relaxation times can be obtained using dynamic parallel plate rheometry. An average melt relaxation time, τ_η, can be extracted from the complex viscosity versus dynamic frequency data using a suitable mathematical representation of the results, such as the simplified Carreau–Yasuda (C–Y) model [26–28], as given by Eq. (1).

$$|\eta^*(\omega)| = \eta_0[1 + (\tau_\eta\omega)^a]^{(n-1)/a} \quad (1)$$

The C–Y model allows three physically meaningful parameters to be obtained from complex viscosity data; the zero shear viscosity, η_0, the average melt relaxation time, τ_η, and an indicator of the breadth of the terminal relaxation, a. For the purposes of this study the value of n will be fixed at 0.18182 in accordance with Graessley's analysis for the linear PE chains [29,30]. Note that the complex viscosity is a function of the oscillatory shearing frequency, ω. Application of the widely accepted, empirical Cox–Merz rule [31] allows one to directly correlate dynamic shear measurements with steady shear behavior, thus making the results of a dynamic experiment relevant to steady state deformation processes. As expected, each of the parameters in the C–Y model are a strong function of the material's MW, MWD, and LCB content. The presence of rheologicaly significant LCBs, defined as branches which are of sufficient length to entangle ($\sim$150 carbons for PE), can be deduced from dynamic rheometry data. Several methods of analysis have been proposed in the literature [32–35]. The semi-empirical method of Janzen and Colby will be applied in this study [32]. This method quantifies LCB content based upon deviations in η_0 from the expected value of a completely linear PE chain of the same MW, as determined by Arnett and Thomas [36].

Generally, it is often possible to use dynamic rheometry to quantify the differences in processability between resins. Specifically, a comparison of the relative tendency of

similar resins to become oriented, and remain oriented, by the process can be made. Thus, it is the goal of this study to describe how the manipulation of melt relaxation time through MW and MWD can influence the final film morphology over a given range of blown film processing conditions. If the resin and process variables are prudently chosen, it should be possible to obtain morphologies that are advantageous to properties such as tear resistance and dart impact.

2. Experimental

Blown films of three gauges (12.5, 20, and 30 μm) were each produced at three different frost line heights (FLHs) (23, 38, and 54 cm) using a high stalk process. The bubble in a high stalk blown film process is characterized by a well defined neck, or 'stalk' region after the die exit which is of approximately the same diameter as the die itself [37–40]. At the top of the stalk, which may be of smaller diameter as a result of draw down, bubble expansion occurs. Following expansion, the molten bubble cools sufficiently to solidify. Therefore, it is important to note that the frost line in this process is found after complete bubble expansion. Overall, the high stalk bubble can be likened in shape to a wine glass. Often times the high stalk process is described as having a delayed blow out when contrasted to the traditional, 'in pocket' bubble configuration. Individual film gauges were achieved by changing the draw down ratio (DDR), (11, 15, and 18) for a constant extruder output and die gap. In all cases the blow-up ratio (final film tube diameter/die diameter) was maintained at 4:1. A 38 mm diameter single screw Davis standard extruder ($L/D = 24$; 2.2:1 compression ratio) fitted with a barrier screw and a Maddock mixing section at the end was used. A 5.1 cm Sano film die with a single lip air ring was used to produce the films. Extruder and die temperatures were set at 210 °C with a 0.90 mm die gap. Extruder output was held constant at 13.2 kg/h.

For each of the above conditions, two HDPE resins were utilized, designated as HDPE-A and HDPE-B. Molecular weight (MW) data was obtained using a waters 150 CV plus gel permeation chromatograph and trichlorobenzene as the solvent at a temperature of 140 °C. Melt rheological measurements were conducted in dynamic oscillatory shear with a parallel plate geometry on a rheometrics RMS-800 at 190 °C. Wide angle X-ray scattering (WAXS) patterns were obtained using a flat plate Warhaus camera with Cu Kα irradiation produced at 40 kV and 20 mA using a Philips tabletop X-ray generator. Two-dimensional small angle X-ray scattering (SAXS) patterns were obtained using the synchrotron source at Brookhaven National Laboratory. Field emission scanning electron micrographs (FESEM) were obtained using a Leo system 1550 at an operating voltage of 2 kV. Samples were prepared for viewing by sputtering with a five nanometer thick layer of platinum/palladium. A Metricon 2010 prism coupler was used to determine the refractive indices of the films in the three principle orthogonal directions: MD, TD, and ND. The average values from these measurements were used to determine the crystalline content by applying the Lorentz–Lorenz equation as discussed by others [41]. The variation in crystalline content between films was found to be small (overall contents 60–63 vol%). Hence, all discussions will consider differences in crystalline content to be negligible.

3. Results and discussion

3.1. Resin characterization

Both the resins used in this study fall into the general category of HDPE resins (pellet densities of 0.949 and 0.950 g/cm^3 for HDPE-A and B, respectively, measured in accordance with ASTM D-1248). Within the class of HDPE resins, variation in MW and MWD can lead to substantial differences in processing characteristics. Noting the values of M_w in Table 1, it can be seen that HDPE-A (368 kg/mol) is of higher MW than HDPE-B (307 kg/mol). The differences in polydispersity index (PDI), calculated in Table 1 for the resins, (19.5 versus 22.0 for HDPE-A and B, respectively) implies there is a small difference in the MWD between the two resins. However, the use of PDI as the sole indicator of MWD can be deceiving, particularly when differences at the high MW end of the distribution are present. Defining an alternative PDI, based on the ratio of the z-average to the weight average MW, yields values of 11.2 for HDPE-A and 6.3 for HDPE-B. This result clearly indicates the presence of a larger fraction of high MW material in the MWD of HDPE-A relative to HDPE-B.

Rheological measurements are very sensitive to the presence of high MW material and LCB, both of which have a substantial impact on processing behavior. As mentioned earlier, a convenient model to quantify the results of complex viscosity versus frequency data is the C–Y model. Table 2 summarizes the C–Y model parameters for both the resins. The viscosity curves from which the data were derived are presented in Fig. 1. At 19.6 s, τ_η is roughly four times greater for HDPE-A relative to HDPE-B, which has a value of 4.8 s. As suggested earlier, the resins' relative ease of processing can be inferred from the dynamic rheology if

Table 1
Molecular weight characteristics of resins. Note that HDPE-A has a greater M_w, M_z and M_z/M_w, suggesting that it contains a greater portion of high molecular weight material than HDPE-B

Resin	M_n (kg/mol)	M_w (kg/mol)	M_z (kg/mol)	PDI (M_w/M_n)	PDI (M_z/M_w)
HDPE-A	19	368	4800	19.5	11.2
HDPE-B	14	307	2180	22.0	6.28

Table 2
Carreau-Yasuda model parameters for resins studied obtained using dynamic parallel plate shear rheometry. Note the substantially longer characteristic terminal relaxation time of HDPE-A relative to HDPE-B

Resin	$\eta_0^\star$ (Pasec)	τ_η (sec)	a
HDPE-A	3.4E + 06	19.6	0.19
HDPE-B	4.9E + 05	4.8	0.30

one assumes the validity of the empirical Cox–Merz rule [31]. The greater average melt relaxation time of HDPE-A implies that, under identical processing conditions, it is more probable for HDPE-A to become oriented in the melt. In addition, HDPE-A will persist in the oriented state for longer times. However, as a single value, τ_η cannot describe the full distribution of relaxation times as it only represents an approximate, number average relaxation time of the melt. An indication of the relative breadth of relaxation times can be ascertained from the C–Y model. The shear thinning transition breadth parameter, a, which is inversely related to breadth of relaxation times, is substantially smaller for HDPE-A. Thus, the value of the breadth parameter is consistent with the GPC data, indicating that the MWD of HDPE-A extends to greater values than that of HDPE-B. Application of the Janzen–Colby theory to diagnose LCB content yields values of 0.020 and 0.008 branching points per 10,000 carbons for HDPE-A and HDPE-B, respectively. These values are extremely low, indicating that both resins are essentially linear.

It is noted that caution must be exercised when extrapolating behavior in shear to large extensional strains. Even within the same resin family, materials that behave similarly under shear may behave quite differently under extension. The presence of LCB and radically asymmetric MWDs are often the confounding factors. The use of the C–Y parameters to contrast the processing behavior here is deemed justifiable because of the high degree of similarity between the resins, as both are highly linear HDPEs. In summary, GPC and rheological measurements determined that HDPE-A is of greater overall MW and has a broader MWD with substantially larger amounts of high MW material than HDPE-B. It is expected that HDPE-A will be more sensitive to process induced orientation than HDPE-B under identical conditions.

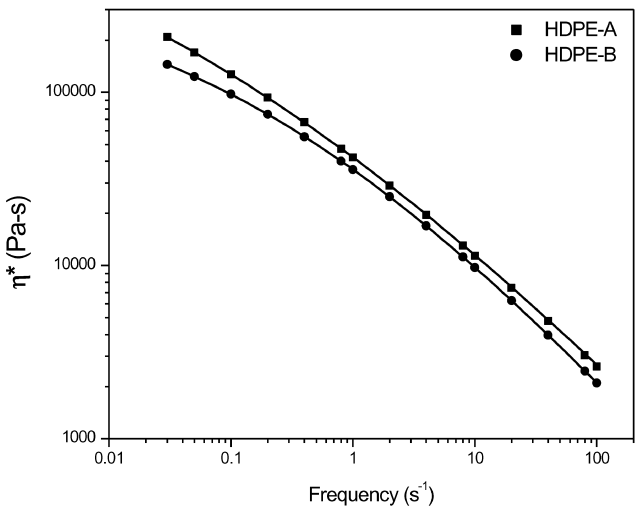

Fig. 1. Complex viscosity determined using dynamic parallel plate shear at 190 C. Solid lines represent C–Y model fitting of data.

3.2. Morphological characterization

3.2.1. WAXS results

The application of WAXS allows one to characterize the orientation state of the crystalline phase. Fig. 2(a) presents the WAXS patterns for the 20 μm HDPE-B films, at each FLH. Fig. 2(b) presents the WAXS patterns for the equivalent films of HDPE-A. It should be noted that the WAXS results presented in Fig. 2 have been obtained at a smaller than customary sample to film distance and with prolonged exposure times to bring out the (020) reflections at the expense of overexposing the more intense (200) and

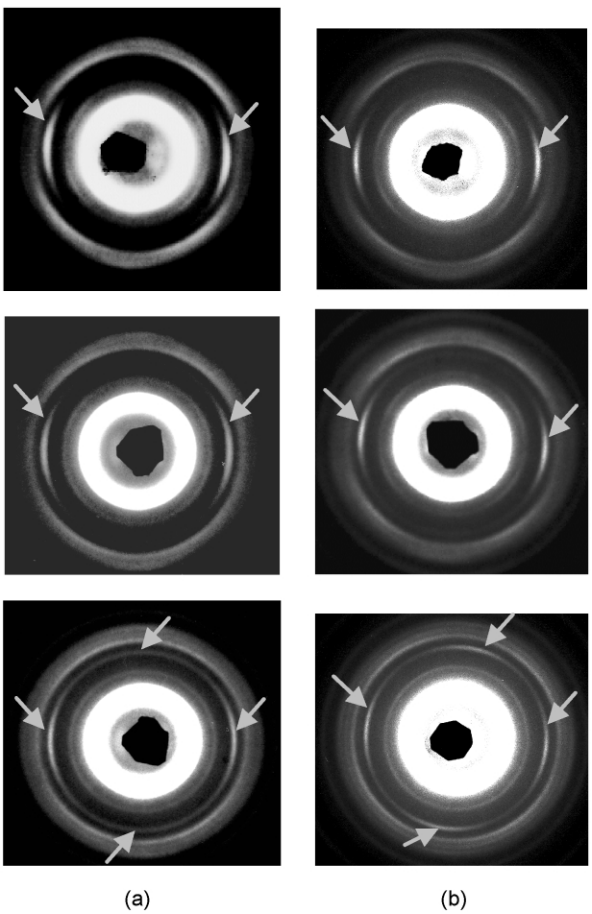

Fig. 2. (a) WAXS patterns of HDPE-B at 20 μm gauge. From top to bottom FLHs are 23, 38 and 54 cm, respectively. Arrows indicate the (020) reflection. MD vertical, TD horizontal. (b) WAXS patterns of HDPE-A at 20 μm gauge. From top to bottom FLHs are 23, 38 and 54 cm, respectively. Arrows indicate the (020) reflection. MD vertical, TD horizontal.

(110) reflections typically noted in PE WAXS patterns. Because a finite time is required for an oriented polymer melt to relax, one expects the amount of MD orientation to decrease, as the FLH is increased, all other processing parameters are held constant. Indeed, at the lowest FLH, 23 cm, the (020) reflection, indicative of the crystalline *'b'* axis, displays a marked dependence of the scattered intensity on the azimuthal angle for both resins A and B. As the FLH increases, the degree of *'b'* axis orientation relative to the MD is seen to decrease.

Of additional note, is the quite striking emergence of a second population of (020) reflections at 90° to the original reflections at the highest FLH that is particularly evident for HDPE-A. The 'four point' WAXS pattern clearly indicates that there are two distinct populations of crystalline material within this film. One population is oriented with the *'b'* axis orthogonal to the MD while the other with the *'b'* axis oriented orthogonal to the TD. Such orthogonally stacked structures have previously been reported by Sue et al. [2] and Dormier [37]. This morphological texture can best be understood in terms of K–M row structures in the perspective of a biaxial deformation process, as originally proposed by Choi et. al [1]. These researchers determined that the biaxial deformation of a PE melt via the blown film process leads to a morphology with row structures oriented within the film plane. The associated fibril nuclei were oriented in various amounts towards either the MD or TD, dependent upon the blow up ratio (BUR) employed. The WAXS patterns of the films in the present study suggest that the high stalk blowing process has induced an extreme example of this biaxial row structure, a morphology in which the row structures are primarily oriented in the film plane along the MD or TD with relatively few row structures oriented at angles between these end points. Such morphologies may be of interest if they are able to simultaneously, restrict the propagation of a tear along the MD and TD directions.

Additional WAXS exposures at each FLH are presented in Fig. 3 for HDPE-B processed to a film gauge of 12.5 μm. Under this set of processing conditions, HDPE-B is observed to produce a combination of the textures noted in Fig. 2. At the lowest FLH in Fig. 3 the *'b'* axis orientation is similar to that of the 20 μm gauge film, with a distinct orientation perpendicular to the MD. However, as the FLH is increased to 54 cm, a four point WAXS pattern similar to that of the HDPE-A, 20 μm gauge film is observed, though with less pronounced azimuthal intensity variation around the (020) reflection. Restated, at a FLH of 54 cm, a second population of crystalline material is introduced which is orthogonal to that formed at the lower FLHs. Thus, the ability to form orthogonal populations of crystalline material is not a property inherent only in HDPE-A, as expected, but is a consequence of the complex interaction between both resin and processing parameters.

3.2.2. SAXS results

While the WAXS results can reveal the presence of a bimodal crystalline orientation, they cannot describe the corresponding structures within which the unit cells exist. Larger structural scale lengths can be probed, with a given wavelength, by studying the scattering behavior at smaller angles. Evidence that these structures are composed of orthogonal stacks of lamellae can be obtained by examining 2D SAXS patterns. As the *'b'* axis is the crystal axis of most rapid chain folded growth in PE, the formation of lamellar structures is such that the *'b'* axis coincides with the long axis of the lamella. If one assumes that the chain and/or unit cell *'c'* axis is perpendicular to the face of the lamellae (i.e. neglects the possibility of chain tilt relative to the lamellar normal), the *'b'* axis of the unit cell will have orientation behavior similar to that of the lamellae. Fig. 4(a),b provide the corresponding SAXS patterns for HDPE-B and HDPE-A, respectively, for the same films presented in Fig. 2(a) and (b). These SAXS patterns provide strong evidence for the presence of bimodal populations of perpendicularly stacked lamellae for the 54 cm FLH, 20 μm gauge HDPE-A and HDPE-B films. Note how the scattered intensity along the equator of these patterns increases from the lowest FLH to the highest. As was the case with the WAXS patterns, the amount of material which is stacked with its lamellar normals parallel to the TD direction increase as the FLH is

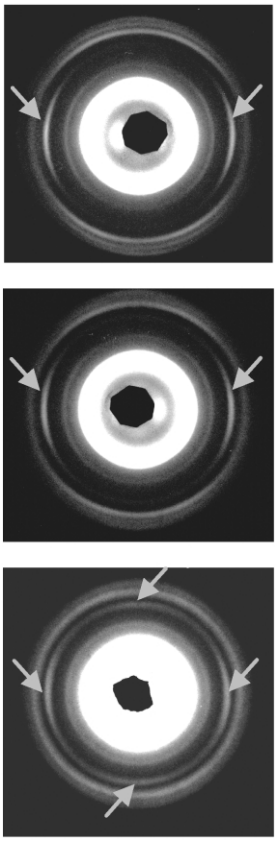

Fig. 3. WAXS patterns of HDPE-B at 12.5 μm gauge. From top to bottom FLHs are 23, 38 and 54 cm, respectively. Arrows indicate the (020) reflection. MD vertical, TD horizontal.

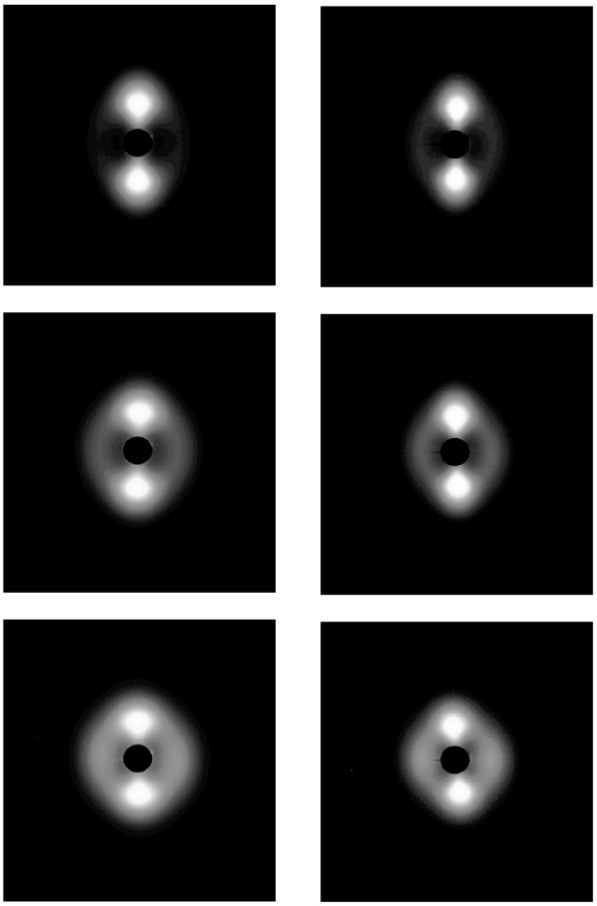

Fig. 4. (a) SAXS patterns of HDPE-B, 20 μm gauge. From top to bottom FLHs are 23, 38 and 54 cm, respectively. MD vertical, TD horizontal. (b) SAXS patterns of HDPE-A, 20 μm gauge. From top to bottom FLHs are 23, 38 and 54 cm, respectively. MD vertical, TD horizontal.

increased, accompanied by a small decrease in the orientation of the MD stacked material.

SAXS patterns for films of HDPE-B processed to a gauge of 12.5 μm are presented in Fig. 5. The SAXS data in Fig. 5 are in direct agreement with the WAXS data of Fig. 3. Increasing the FLH leads to the formation of lamellae stacked perpendicular to the TD. Excellent correlation between the presence of the *'b'* axis reflection along the WAXS meridian and the lamellar reflection along the SAXS equator is found for this set of films, as well as for the others already discussed. Differences in the relative amounts of TD stacked material, between resins, will be addressed later in the discussion section.

Comparing the positions of the maxima in the radial scattering angle for the MD and TD populations observed in the SAXS patterns indicates that the average long spacing between lamellar centers is approximately equivalent for all of the films studied. Additionally, DSC traces (not shown) of these films did not resolve two distinct melting peaks, signifying that both the populations, within a given film, consist of lamellae with very similar melting behavior.

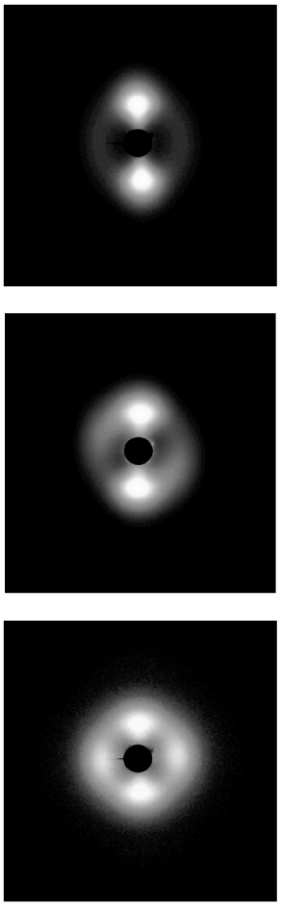

Fig. 5. SAXS patterns of HDPE-B, 12.5 μm gauge. From top to bottom FLHs are 23, 38, and 54 cm, respectively. MD vertical, TD horizontal.

Furthermore, the breadth of the melting transition, as measured by DSC, was consistent, regardless of the resin or processing conditions used to produce the film. This is a secondary indicator of the equivalence of their lamellar thickness distributions.

3.2.3. FESEM results

The orientation of lamellae at the film surface was characterized directly by FESEM. Two representative images are provided in the micrographs of Fig. 6. These surface features match very well with the previous SAXS patterns. At the lowest FLH, the morphology is dominated by stacks of lamellae oriented perpendicular to the MD. At the highest FLH, two distinct populations of lamellae can be observed, one perpendicular to the MD, the second perpendicular to the TD. It was difficult however, to quantify the degree of interdigitation and/or distribution of perpendicular lamellae from the FESEM results. Despite this, the FESEM results do visually confirm the presence of orthogonal stacks of lamellae at the surface, in harmony with the bulk structure determined by WAXS and SAXS.

3.2.4. Additional WAXS results

The data from the previous sections have demonstrated

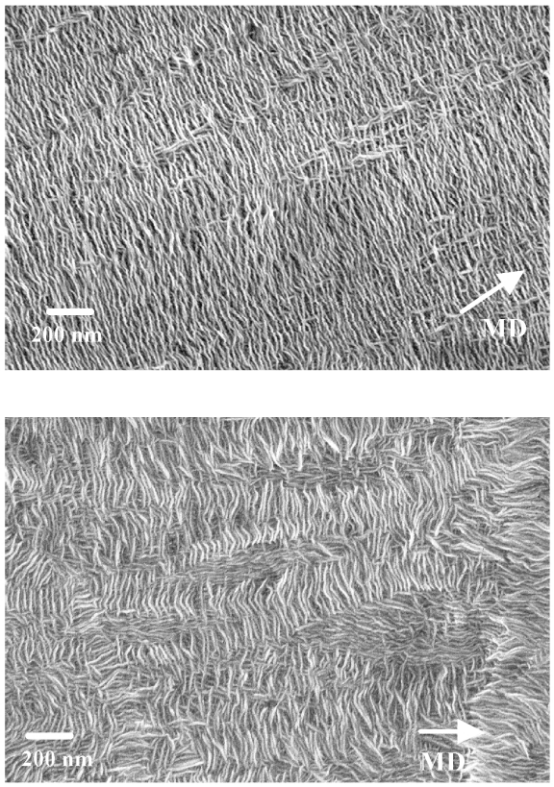

Fig. 6. FESEM micrographs of HDPE-A. Film gauge 20 μm FLHs of 23 and 54 cm, respectively.

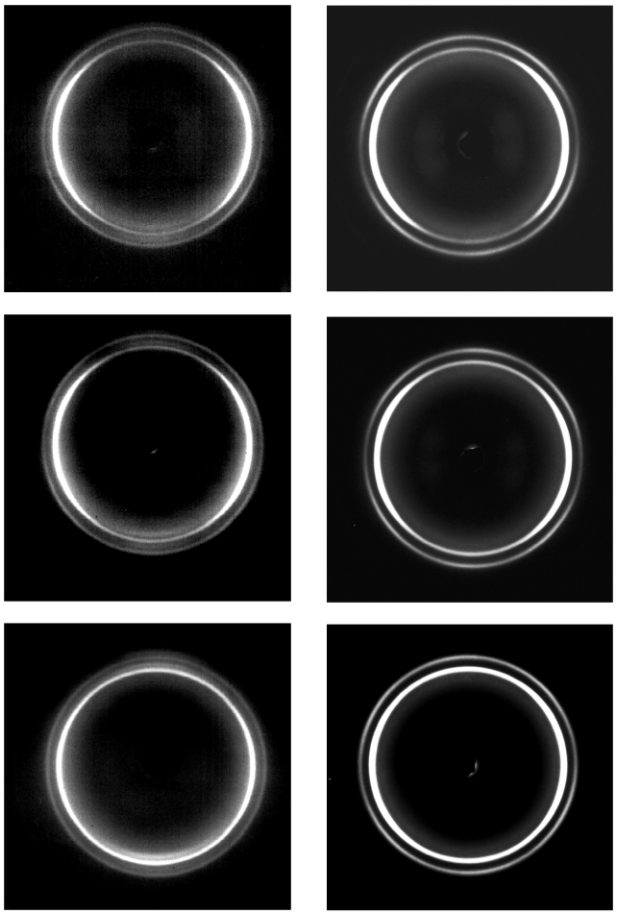

Fig. 7. (a) WAXS patterns of HDPE-B at 20 μm gauge. From top to bottom FLHs are 23, 38, and 54 cm, respectively. Arrows indicate the (020) reflection. MD vertical, TD horizontal. (b) WAXS patterns of HDPE-A at 20 μm gauge. From top to bottom FLHs are 23, 38, and 54 cm, respectively. Arrows indicate the (020) reflection. MD vertical, TD horizontal.

that by varying the FLH, for a given set of processing conditions, it was possible to develop unimodal or bimodal orientation states of the lamellae. To gain further insight into the conditions which gave rise to these structures, examination of the diffraction behavior from the (110) and (200) planes of these films is useful. Fig. 7(a) and (b) present WAXS patterns of the (110) and (200) reflections for HDPE-B and HDPE-A, respectively, processed to a 20 μm gauge. These more conventional WAXS patterns presented in Fig. 7(a) and (b) were obtained at a greater sample to film distance, and exposed for shorter times than those shown in previous figures, allowing the details of the (110) and (200) reflections to be observed at the expense of the (020) reflection. It can be noted from the split nature of the (110) and (200) reflections, and the preference for the (200) reflection to position itself perpendicular to the MD for the 23 and 38 cm FLHs in both sets of films, that the crystallization conditions fall into the intermediate stress regime of the K–M model. This result suggests that the chain axis in these populations of lamellae were well aligned with their respective nucleating fibril at the time of crystallization. In Fig. 7(a) and (b) at the highest FLH studied, 54 cm, both films display an increase in scattered intensity along the meridian. This is anticipated, based on the (020) WAXS as well as SAXS results, and arises from the formation of TD stacked material. However, it should be noted that the (200) scattering resulting from the TD population of lamellae takes the form of a single arc (i.e. not split), perpendicular to the TD direction. This indicates that the TD stacked material formed under conditions of high stress according to the K–M model. Furthermore, it is of interest to note that the (200) diffraction due to MD stacked lamellae in the HDPE-A films retains the intermediate stress pattern, a split arc, at all FLHs, while the (200) reflection in the HDPE-B film becomes increasingly uniform with increasing FLH. The behavior of the (200) reflection, thus suggests that the MD and TD lamellar stacks are formed under different stress conditions, and differences in the relaxation behavior of the two resins can be noted by the manner in which they crystallize. Indeed, it is important to note that the bubble cools as it travels from the die to the frost line; therefore, the rate of molecular relaxation decreases over this distance. Because of this, stresses and orientation induced during the second deformation event, bubble expansion, will decay more slowly in comparison to those developed during the first deformation event, MD draw in the stalk region.

3.3. Formation of orthogonal stacks

From the above results it can be well appreciated that the differences in both resin and processing variables can have a dramatic effect on the structure of the film. The influence of FLH on the orientation of the MD stacked material can be readily explained by the K–M model and relaxation behavior. Increasing the FLH allows greater time for the relaxation of MD oriented chains before crystallization, thus lowering the number of MD oriented fibril nuclei and the associated level of crystalline orientation. This phenomenon is demonstrated by the decreased azimuthal dependence of the (020), and to a lesser extent the (200), reflections as the FLH is increased. Note that this effect is independent of the bubble expansion step. Indeed, the high stalk configuration can be considered a sequential deformation process, with an initial stretch along the MD in the neck region, soon followed by a second stretch along the TD due to bubble expansion. Comparisons with the biaxial tentor frame process may not be applicable, since solidification occurs between the MD and TD stretching events in contrast to the blown film process.

The orientation state of the MD stacked lamellae also demonstrates the inherent differences in melt relaxation behavior between the two resins. Recall from the rheology results that HDPE-A, containing a greater fraction of high MW chains, relaxes substantially slower than HDPE-B. Comparisons of the (200) reflections from the MD stacked lamellae demonstrated that films produced at the lowest FLH (i.e. most rapidly quenched), were indicative of an intermediate stress condition for both resins. While the films produced using HDPE-A retained the split (200) reflection along the equator at all FLHs studied, the (200) reflection became uniform along the equator for HDPE-B at the highest FLH. This clearly suggests that the level of MD chain orientation decayed more rapidly in the stalk region for HDPE-B relative to HDPE-A. Thus, it appears under the conditions studied, that the degree of orientation of the MD stacked material is determined largely by the relaxation behavior. This is not surprising as the high stalk process inherently provides time for partial relaxation of MD orientation prior to solidification.

As stated earlier, the differences in rheological behavior between the two resins, primarily due to variation in MWD, affects not only their relative relaxation behavior, but also the levels of stress which develop in the bubble during processing. These stresses have a profound impact on the final morphology and are key to understand its formation. When producing film utilizing the high stalk configuration, the diameter of the stalk region is commonly observed to decrease slightly prior to the bubble inflation point. The magnitude of this reduction in stalk diameter is proportional to the stress level in the melt. Material and process variables, which promote greater stresses in the melt, lead to a greater decrease in the stalk diameter prior to expansion. This phenomenon is shown schematically in Fig. 8. It is recognized that the reduction in stalk diameter in turn results in an 'effective' BUR which is greater than the macroscopic BUR, which can be defined as the ratio of final bubble diameter to die diameter. Therefore, resins or processing conditions, which promote greater stresses, result in an increased effective BUR. A greater effective BUR should lead to increased TD orientation.

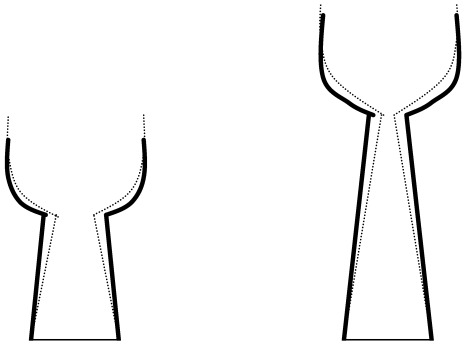

Fig. 8. Effect of increasing FLH on bubble shape. Note that as the FLH increases (left to right) the effective BUR increases. Dark lines and dashed lines represent bubble shape of lower stress and higher stress processing conditions, respectively, at equivalent FLHs. Higher cm, (▼)—FLH = 54 cm.

It is reasonable to expect for these highly similar resins, based on HDPE-A's higher viscosity, that it will generate greater stresses in the melt during fabrication, relative to HDPE-B. Recall that this trend was evident in the behavior of the (200) WAXS reflections of Fig. 7(a) and (b). These higher stresses should result in a greater effective BUR. Indeed, the WAXS patterns of Fig. 2(a) and (b) and SAXS patterns of Fig. 4(a) and (b), which compare the two resins under identical processing conditions, show that the HDPE-A film at the greatest FLH has more TD stacked material. Thus, differences in melt stress arising from the resins MW and MWD clearly affect the end morphology.

The two process variables examined also influence the stress levels present. Obviously, increasing the DDR will increase the level of processing stress. This will lead to a greater reduction in stalk diameter, which in turn should produce a larger population of TD stacked material. Comparing the intensity of scattering arising from TD stacked material in Figs. 2(a) and 3 (WAXS) and Figs. 4(a) and 5 (SAXS), it is apparent that increasing the DDR (down gauging) produced a larger fraction of TD stacked material. In addition, it is typically observed that the stalk diameter decreases with increasing FLH. That is, the longer the stalk region, the greater is the narrowing of the stalk prior to expansion. In accordance with this observation, it is expected that the amount of TD stacked material will increase as the FLH is raised. In all instances, the WAXS, SAXS, and FESEM data presented show that this is clearly the case.

3.4. Mechanical properties

3.4.1. Elmendorf tear

As stated earlier, a film morphology consisting of

perpendicular stacks of MD and TD lamellae has the potential to strongly influence tear resistance. Ideally, orthogonal stacks of crystalline material will be situated so as to resist the propagation of tears along both the MD and TD. The results of Elmendorf tear experiments conducted in accordance with ASTM D-1922 along the film MD are presented in Fig. 9. These results are plotted as a function of film gauge and thus are not normalized on film thickness. Thicker films produce greater tear resistance values, as expected, due to the greater amount of material being tested. The MD tear resistance is observed to increase as the FLH is increased for constant gauge. It is well known that a high degree of chain orientation along the MD leads to poor tear resistance along the MD. This is because tear propagation parallel to the chain backbone requires less energy than propagation perpendicular to the chain. Thus, those films which have the greatest degree of orientation relative to the MD show the poorest MD tear resistance.

Results concerning the resistance to the propagation of a tear initiated along the TD, an Elmendorf tear test along the TD, are presented in Fig. 10. Again, as the results are plotted as a function of film gauge, they are not normalized on thickness. The trend in tear resistance as a function of FLH is opposite to that found in the MD direction, as expected. Those films, which have the highest degree of MD orientation, while unable to resist tear propagation along the MD, have an enhanced ability to resist tear propagation along the TD. Those films processed with the lowest FLH, and thus containing the greatest amount of MD orientation, have the greatest TD tear resistance at a constant gauge. The Elmendorf tear results suggest that for a given BUR and MD, it may not be easily possible to improve tear resistance in one direction without compromising properties in the orthogonal direction.

3.4.2. Dart impact

As noted above, the resistance to tear in a given direction can be improved by increasing the level of chain orientation perpendicular to that direction. Because this orientation produces poorer tear resistance in the orthogonal direction, a trade off is inherent in the process. This poses an interesting question as to what changes will occur when a film is tested in a biaxial deformation mode. The results of dart impact tests conducted according to ASTM D-1709 (method A) are provided in Fig. 11. As with the tear results, the dart impact resistance is plotted as a function of film gauge. While HDPE-A shows the intuitive result, that impact resistance increases with film thickness, the same is not true for HDPE-B. The dart impact resistance increases as the film gauge is decreased for HDPE-B over this set of processing conditions. It can also be noted from Fig. 11 that the impact resistance of HDPE-A and HDPE-B films increases with FLH, implying that a more balanced orientation state leads

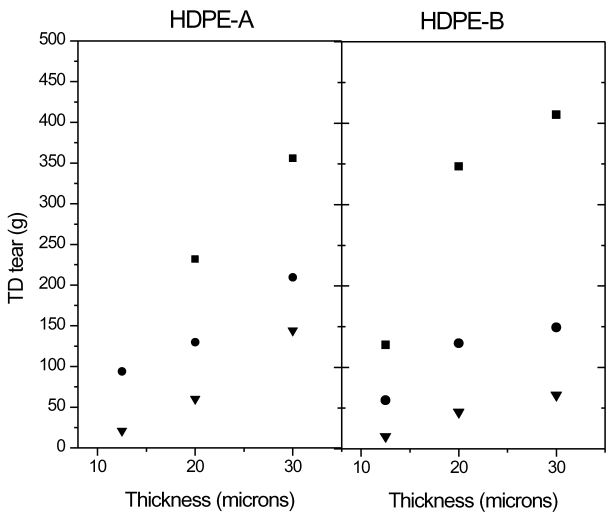

Fig. 10. Elmendorf tear results. Test conducted along film TD. (■)—FLH = 23 cm, (●)—FLH = 38 cm, (▼)—FLH = 54 cm; stress conditions may be induced by the process variables (increase DDR) or material variables (higher viscosity resin).

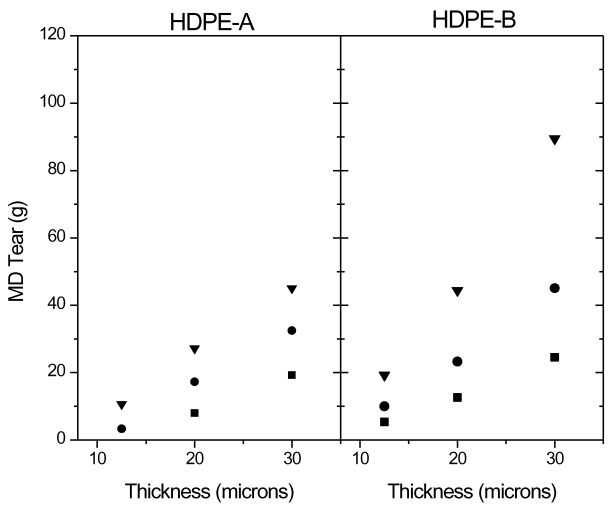

Fig. 9. Elmendorf tear results. Test conducted along film MD. (■)—FLH = 23 cm, (●)—FLH = 38.

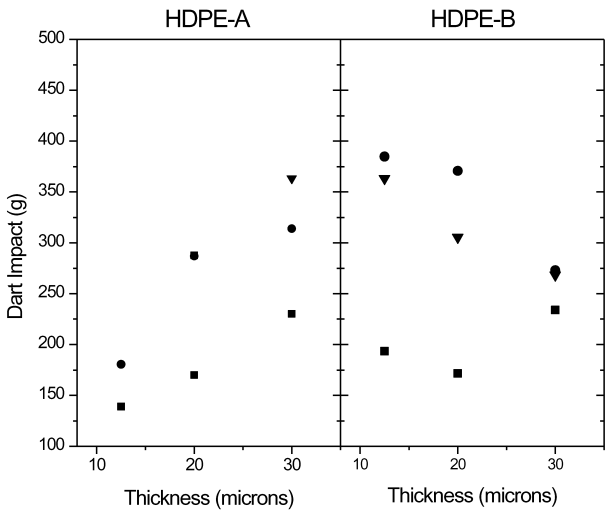

Fig. 11. Dart impact properties. (■)—FLH = 23 cm, (●)—FLH = 38 cm, (●)—FLH = 54 cm.

to an enhancement of this property. It is not understood at this time what role the differences in morphology noted by the (200) reflection may have on the dart impact behavior. Additionally, differences in amorphous orientation and tie chain density, not quantified in this study, may influence the behavior as well. These results as well as those of others, suggest the need for further systematic studies of dart impact behavior as a function of processing conditions for well characterized resins and film morphologies.

4. Conclusions

Films with orthogonal row structures were produced using the high stalk blown film configuration for two resins at varying FLH and DDR. The HDPE resins utilized were highly linear, differing in MW and MWD. The relative amounts of MD versus TD oriented crystalline material were found to depend strongly on the FLH and the stress levels generated during the process. Higher FLHs led to a greater proportion of TD oriented row structures in all instances. The orientation of the MD stacked material was reasoned to be a function of the MWD and the time given for relaxation in the stalk, as controlled by the FLH. The reduction in stalk diameter prior to inflation, due to stresses within the stalk, caused the effective BUR to be greater than the BUR of 4:1, conventionally defined by the die and final bubble diameter. The amount of TD stacked material was found to be dependant upon this effective BUR. Processing and resin variables which resulted in greater stress increased the effective BUR, resulting in larger fractions of TD stacked material. Elmendorf tear resistance was found to increase in the MD and decrease in the TD with increasing FLH. Thus, the tear properties were observed to be a strong function of the molecular anisotropy of the film. Finally, an intriguing effect, the increase in dart impact resistance with down gauging, was noted for HDPE-B.

Acknowledgements

The Virginia Tech authors would like to thank Chevron Phillips Chemical Company for funding and collaborations.

References

[1] Choi K, Spruiell J, White J. J Polym Sci, Polym Phys 1982;20:27.
[2] Sue HJ, Lu J, Rieker TP. Polymer 2001;42:4635.
[3] Krishnaswamy RK, Sukhadia AM. Polymer 2000;41:9205.
[4] Desper CR. J Appl Polym Sci 1969;13:169.
[5] Maddams WF, Preedy JE. J Appl Polym Sci 1978;22:2721.
[6] Maddams WF, Preedy JE. J Appl Polym Sci 1978;22:2739.
[7] Maddams WF, Preedy JE. J Appl Polym Sci 1978;22:2751.
[8] Hofmann D, Geiss D, Janke A, Michler GH, Fieldler P. J Appl Polym Sci 1990;39:1595.
[9] Lindenmeyer PH, Lustig S. J Appl Polym Sci 1965;9:227.
[10] Gilber M, Hemsley DA. Br Polym J 1987;19:9.
[11] Patel RM, Butler TI, Walton KL, Knight GW. Polym Engng Sci 1994; 34(19):1506.
[12] McRae MA, Maddams WF. J Appl Polym Sci 1978;22:2761.
[13] Ashizawa H, Spruiell JE, White JL. Polym Engng Sci 1984;24(13): 1035.
[14] Huck ND, Clegg PL. SPE Trans 1961;July:121.
[15] Pazur RJ, Prud'homme RE. Macromolecules 1996;29:119.
[16] Lin L, Argon AS. J Mater Sci 1994;29:294.
[17] Butler MF, Donald AM. J Appl Polym Sci 1998;67:321.
[18] Zhou H, Wilkes G. Polymer 1998;39:3597.
[19] Lee SY, Basset DC, Olley RH. J Mater Sci 2000;35:5101.
[20] Ward IM. Structure and properties of oriented polymers. London: Chapman and Hall; 1997.
[21] Keller A, Machin MJ. J Macromol Sci 1967;B1:41.
[22] Keller A, Kolnaar JWH. Prog Colloid Polym Sci 1993;92:81.
[23] Keller A, Odell JA. Colloid Polym Sci 1985;263:181.
[24] De Gennes PG. J Chem Phys 1974;60(12):5030.
[25] Smith DE, Babcock HP, Chu S. Science 1999;283:1724.
[26] Rohlfing DC, Janzen J. Melt rheological characterization of metallocene-catalyzed polyethylenes. In: Scheirs J, Kaminsky W, editors. Metallocene-based polyolefins. Chichester, UK: Wiley; 2000.
[27] Hieber CA, Chiang HH. Rheologica Acta 1989;28:321.
[28] Hieber CA, Chiang HH. Polym Engng Sci 1992;32:931.
[29] Graessley WW. J Chem Phys 1967;47:1942.
[30] Graessley WW. Advd Polym Sci 1974;16:1.
[31] Bird RB, Armstrong RC, Hassager O, Dynamics of polymeric liquids, vol. 1. New York: Wiley-Interscience; 1987.
[32] Janzen J, Colby R. J Mol Struct 1999;486:569.
[33] Wood-Adams P, Dealy J. Macromolecules 2000;33:7481.
[34] Shroff R, Mavridis H. Macromolecules 1999;32:8454.
[35] Shroff R, Mavridis H. Macormolecules 2001;34:7362.
[36] Arnett R, Thomas C. J Phys Chem 1980;84:649.
[37] Dormier EJ, Brady JM, Chang WH, Barnes JD, Schregenberger SD. SPE Antec Conf Proc 1989;696.
[38] Shirodhkar PP, Schregenberger SD. SPE Antec Conf Proc 1987;37.
[39] Detter CV. Plast Engng 1982;29.
[40] Wooster JJ, Cobler BA. SPE Antec Conf Proc 1995;20.
[41] Pepper RE, Samuels RJ. Refractometry. In: Mark HF, Bikales NM, Overberger CG, Menges G, editors. Encyclopedia of polymer science and engineering, vol. 14. New York: Wiley; 1998. p. 261.